Slag and Thermal Environment of a Spinning Rocket Motor

I-Shih Chang*
The Aerospace Corporation, El Segundo, California 90009

The effect of slag in the chamber on the motor-case thermal environment of a spinning rocket motor is studied. Very good agreement between analysis results and ground test data is obtained for motor-case temperature histories throughout the motor firing and heat-soak period of the spinning payload assist module (PAM) (Star-48) qualification motors. In the area in which the insulation is exposed to combustion products during motor firing, the insulation erosion rate is a function of motor spinning rate. During heat soak, the slag mass is considered to be the single parameter that influences the thermal environment of a spinning rocket motor. Available data from a flight motor are analyzed and compared with the analysis results. The thermal environment for the PAM-S/Ulysses flight motor is predicted. For a spinning flight motor, the analysis reveals that the insulation erosion rate and the amount of slag in the chamber of a spinning flight motor can be assessed or sensed from monitoring the temperature history on the outside surface of the motor case.

Nomenclature

g	= acceleration of gravitational force, 32.2 ft/s^2 (9.8 m/s^2)
NQ2, Q2, Q5, Q6, Q7	= designations for qualification motors
q_0	= reference soak-out radiation heating rate, Btu/s-ft^2 (cal/s-cm^2)
q	= soak-out radiation heating rate, Btu/s-ft^2 (cal/s-cm^2)
T_{max}	= maximum motor-case temperature, °F (°C)

I. Introduction

IT has been demonstrated in ground tests and observed from flight motor performance data that an increase in radial and/or axial acceleration results in an increase in the amount of slag accumulated in the chamber of a motor with a submerged nozzle design. The slag is composed of aluminum and alumina (Al_2O_3) residue from the combustion of aluminized solid propellant. The presence of slag in the chamber influences motor burnout weight, soak-out thermal environment, residual thrust, and motor performance.[1] An excessive amount of slag in the chamber also could impact mission success. It has been postulated[2] that overheating of the motor case and loss of structural rigidity around the nozzle contributed to the notorious nutational instability (coning) associated with a spinning flight motor, as a result of slag accumulation in the motor chamber.

From a space-vehicle performance standpoint, the maximum amount of slag allowed to be accumulated in the motor chamber is limited by the motor payload delivery capability and by the ability of the onboard nutation control system to correct vehicle wobbling, since slag has been considered[3] to be one of the factors that could contribute to vehicle coning. For example, a slag mass of 44 lb (20 kg) has been established as the maximum allowable amount of slag in the payload assist module (PAM) motor chamber that can be tolerated by the PAM-S/Ulysses mission. However, different methodologies yield different amounts of slag in the chamber of a flight motor. The slag masses ranging from 1 to 70 lb (0.45–31.8 kg) have been predicted by different analysts[4] for the PAM-S/Ulysses mission. But no spinning flight space motor has been recovered to provide a slag data base for quantitative comparison.

It is the intent of this paper to address the effect of slag accumulated in the chamber on the thermal environment of a spinning PAM (Star-48) motor. A thermal model is developed for this purpose. In the area in which the insulation is covered by propellant during motor firing, the soak-out thermal environment is determined by the amount of slag accumulated in the motor chamber. In the remaining area of the motor case, in which the insulation is exposed to hot combustion products, the thermal environment is determined by the motor spinning rate during motor firing (which affects insulation erosion rate) and by the amount of slag retained in the chamber during heat soak. Based on extrapolation of the slag radiation heating level derived from the ground qualification motor test data, the thermal environments corresponding to various in-flight slag masses can be calculated. Recorded data on the aft dome of a previously flown PAM motor are analyzed and compared with the analysis results. The thermal environment of the spinning PAM-S motor for the Ulysses mission is predicted and presented. Utilization of temperature history on the outside surface of the motor case to assess the insulation erosion rate and the amount of slag accumulated in the chamber of a flight motor is discussed.

II. PAM-S/Ulysses Mission Overview

To propel spacecraft from low Earth orbit into final orbit, the Ulysses mission (solar polar orbit via Jupiter) adopts the nonspinning, inertial upper stage (IUS), two-stage, solid rocket motors; it also uses a PAM-S free-spinning, solid rocket motor. The PAM-S/Ulysses is scheduled to be launched in October 1990. Because of low spacecraft weight and, hence, high peak axial acceleration during motor firing, separation of the Ulysses spacecraft from the PAM-S (Star-48B motor) payload adapter (see Fig. 1) is delayed until 510 s after motor burnout (600 s from ignition). This is done in order to avoid recontact between the spacecraft and the expended stage due to the presence of residual thrust in the motor. The residual thrust comes from pyrolysis gas generated from heat soak of the motor-case insulation. The extent of heat soak is influnced by the temperature of the nozzle block, the amount of residual combustion products, and slag retained in the chamber after motor burnout. The PAM-S motor shown in Fig. 2 is to be spun at 72 rpm with a "free-spin" gas-generator system.[5] The

Received May 12, 1990; presented as Paper 90-2205 at the AIAA/ASME/SAE/ASEE 26th Joint Propulsion Conference, Orlando, FL, June 16–18, 1990; revision received Oct. 26, 1990; accepted for publication Oct. 26, 1990.

*Senior Engineering Specialist, Vehicle and Control Systems Division. Member AIAA.

peak axial acceleration reaches 11.1 g, which is much higher than a typical PAM-D (Star-48) flight motor (4.5 g). The PAM-S motor is identical to the PAM-D motor, except for a 30-lb (13.6-kg) increase in propellant load and a carbon/phenolic exit cone (see Fig. 3) instead of a two-directional (2-D) carbon/carbon exit cone.

III. Correlation and Analysis

The thermal model based on the charring and material ablation (CMA) program[6] was developed under this study to compute the temperature of the PAM motor case. The thermal model considers silica-filled ethylene propylene diene monomer (EPDM) rubber insulation charring, variable material thermal properties for both rubber and titanium, and time-dependent radiation heating from nozzle block and slag. Although the CMA program is used extensively in industry, its application to rubber material is infrequent, primarily because of the lack of kinetic reaction constants and pyrolysis gas enthalpy data for rubber-charring process simulation. The material properties shown in Ref. 7 provide adequate information for the present EPDM charring and material ablation analysis. The PAM titanium motor-case thickness is 0.069 in. (0.175 cm); the EPDM-insulation thickness varies from 0.04 in. (0.1 cm) at the forward dome to 0.40 in. (1.0 cm) at the aft dome. Table 1 summarizes the PAM static test motors considered in this paper. The temperature measurement locations at the forward, mid, and aft domes of the PAM qualification motors, used for present analysis comparison, are noted in Fig. 2. The boundary conditions for the CMA thermal model are discussed in the following subsections.

A. Backwall Surface Boundary Condition

A radiation-cooling boundary condition with 0.2 emissivity and reservior temperature at ambient condition (60°F) (16°C) is applied on the backwall surface of the bare titanium without the multilayer insulation (MLI) blankets to cover the outside surface of the motor case. When the motor case is covered with MLI blankets, an adiabatic boundary condition is applied on the titanium backwall surface of the thermal model. The analysis results indicate that the adiabatic backwall boundary condition gives a peak temperature approximately 40°F (22°C) higher than that of the radiation cooling boundary condition during heat soak. Since the PAM qualification motors were tested without MLI, the results of analysis with the adiabatic boundary condition will not be shown in this paper. Note, however, the MLI covers the outside surface of the motor case on the flight motor. Also, the predicted peak motor-case temperature for a flight motor needs to be increased by 40°F (22°C), to account for the difference between radiation-cooling and adiabatic backwall boundary conditions.

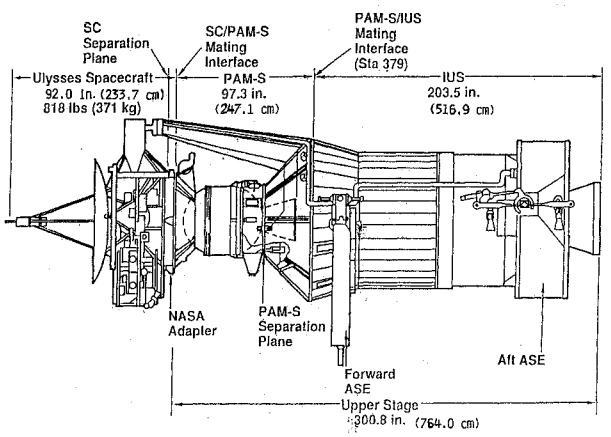

Fig. 1 Ulysses/PAM-S/IUS configuration.

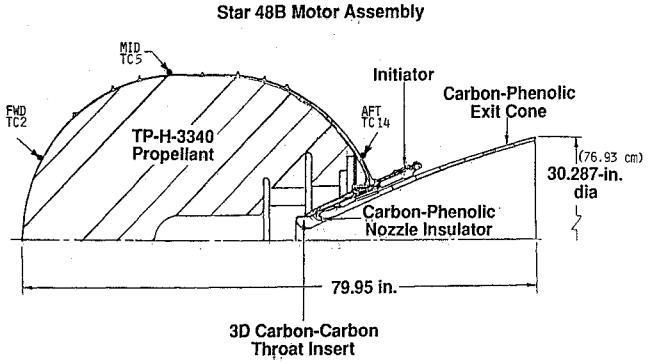

Fig. 2 PAM-S/Ulysses solid rocket motor.

B. Heated Surface Boundary Condition (During Motor Firing)

For a nonspinning ground motor, since particle-to-gas volume fraction is small (less than 0.001), spotty contact occurs between alumina particles and the EPDM charred eroding surface during motor firing. The temperature on the EPDM charred eroding surface is set at 1500°F (816°C); the temperature was obtained from an arcjet test conducted during the IUS anomaly investigation in 1984[8] and provides good results for insulation design of nonspinning motors.

For a spinning ground motor, continous shearing contact between alumina particles and EPDM charred eroding surface dictates that a particle surface solidification temperature (3720°F) (2049°C) be imposed on the EPDM heated surface throughout the duration of motor firing. Although the temperature of molten alumina particles in the chamber is at 6000°F (3316°C), the particle surface solidification occurs immediately after the molten particles surface comes in contact with a cooler (1500°F) (816°C) EPDM pyrolysis gas layer; motor spinning sustains this continuous contact between the EPDM charred eroding surface and the solidified surface of alumina particles.

In addition, for a spinning ground motor, the slope of the recorded temperature vs the time curve on the outside surface of the motor case at the end of burn is used to derive the insulation erosion rate during motor firing. This is done iteratively through trial and error. The CMA thermal model is run and a serach for an analysis EPDM erosion rate is conducted. This produces the slope of temperature vs the time curve on the outside surface of the motor case in agreement with the measured value at the end of burn. In the area in which insulation is exposed to hot combustion products during motor firing, the duration of exposure needs to be defined from motor ballistics analysis. On the aft dome of the PAM motor shown in Fig. 2, full duration of exposure throughout motor firing occurs on the insulation's heated surface.

Based on the iterative method discussed above, Fig. 4 shows the derived EPDM erosion rates from the present analysis as a function of motor rpm on the aft dome of the PAM qualification motors (Table 1). Shown in the same figure are the slag masses at different spinning rates from the ground motor tests. For motors with chamber and grain design different from those of the PAM motor, the relationship between the

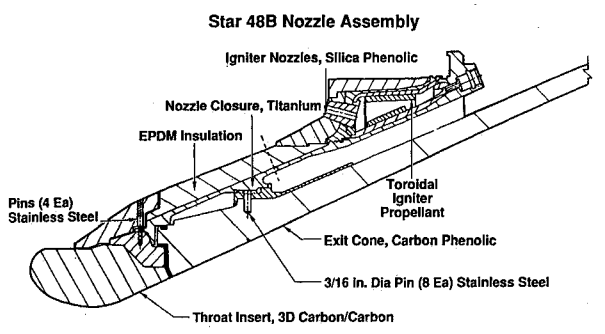

Fig. 3 PAM-S/Ulysses solid rocket motor nozzle.

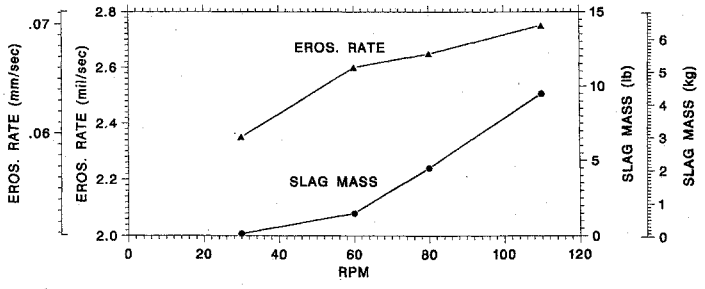

Fig. 4 Aft-dome erosion rate.

Table 1 Star-48 static test motors

	Q2	Q7	Q5	NQ2	Q6
Action time, s	77.76	83.89	71.77	84.46	82.89
Propellant temperature, °F (°C)	30 (−1)	75 (24)	110 (43)	92 (33)	110 (43)
Revolutions per minute, rpm	30	60	75	80	110
Slag, lb (kg)	0.14 (0.06)	1.5 (0.7)	4.5 (2.0)	4.5 (2.0)	9.5 (4.3)

insulation erosion rate and the motor spinning rate may not be the same as that given here; but it can be derived similarly from the motor test data. This paper, nevertheless, illustrates a method of evaluating insulation thickness at the end of motor firing, based on the temperature information recorded on the outside surface of the motor case from an EPDM charring and material ablation thermal analysis.

Normally, the insulation erosion rate derived from the analysis can be compared with the measured post-test insulation thickness if the motor is quenched to preserve the insulation condition at the end of burn. Unfortunately, no part of the PAM qualification motor was quenched at the end of burn and the measured post-test insulation thickness compiled in Ref. 9 is not reliable. For example, on the aft dome, the maximum soak-out temperature of the PAM qualification motors reaches between 350°F (177°C) for the Q2 motor and 500°F (260°C) for the Q6 motor, which exceeds the allowable bondline temperature; debond between the EPDM insulation and the titanium motor case necessarily occurs. This explains why the measured post-test case insulation thickness varies significantly at different azimuthal locations with the same radial distance. This also explains why the measured post-test case insulation thickness is much greater, in some instances, than the pretest thickness.

C. Heated Surface Boundary Condition (During Heat Soak)

During heat soak, the radiation heating rate from the nozzle and slag to the motor case needs to be established. The radiation emitted from the nozzle assembly decreases (monotonously) after motor burnout. The radiation heating rate from the slag to the motor case drops considerably as molten slag surface temperature decreases, stays nearly constant (3720°F, 2049°C) at liquid-to-solid phase transition, and settles to an equilibrium value. This physical reasoning essentially dictates, qualitatively, the required curve shape of the time rate change of the soak-out radiation heat flux. The quantitative, time-dependent, radiation heat flux is derived, iteratively, from correlating (or matching) computed temperature from the CMA thermal model with the measured temperature obtained from a reference ground motor test. No good agreement between analysis result and measured temperature data can be obtained, if a constant radiation heating rate is used or a non-charring analysis is performed, such as that accomplished in Refs. 10 and 11.

On the forward dome and a portion of the mid-dome of the PAM motor shown in Fig. 2, the insulation is covered by the propellant and is not exposed to hot combustion products until all of the propellant has been consumed. There is no EPDM insulation erosion in this region from the present thermal model. Only the heated surface boundary condition during heat soak, as discussed previously, needs to be imposed on the insulation heated surface. In this paper, the measured temperature data from the Q2 motor [30 rpm, 0.14-lb (0.06-kg) slag] are used to derive the reference radiation heating rates during heat soak at forward-, mid-, and aft-dome stations of the PAM motors shown in Fig. 2. On the aft dome, where the insulation is exposed to combustion products, the heated boundary condition during motor firing needs to be imposed on the eroding EPDM heated surface before the soak-out heated boundary condition is applied to the thermal model on the aft dome. These time-dependent reference radiation heating rates, which provide a good match between the computed temperature and the measured temperature on the outside surface of the Q2 motor case, are shown in Fig. 5.

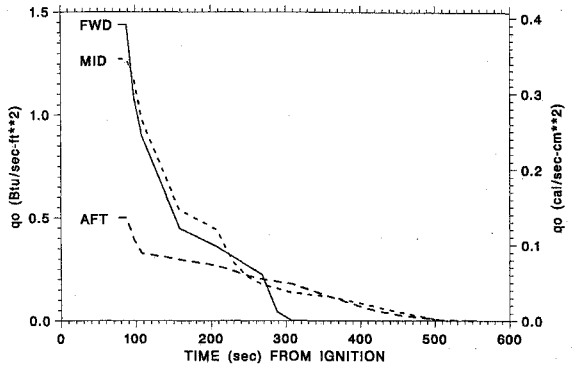

Fig. 5 Q2 motor soak-out radiation heating rate.

For a motor spinning at a different rpm than that of the reference Q2 motor, the radiation heating rate is obtained from multiplying the reference radiation heating rate by a constant enhancement factor, representing the effect of increasing (or decreasing) the amount of slag in the chamber, without changing the shape of the reference time-dependent, radiation heating rate curve. This is tantamount to directly relating the chamber thermal environment to one single parameter, namely, the amount of slag retained in the chamber during heat soak. Consequently, the amount of effort spent in correlating the temperature data obtained from various ground motors can be reduced significantly. It will be shown in Sec. IV that this approach works well for the motors considered in this study.

Figure 6 shows the soak-out radiation heating enhancement factor as a function of slag mass derived from this method for the PAM qualification motors of Table 1. Once the soak-out radiation heating rates for the ground motors have been established from test data correlation, the soak-out thermal environment of a spinning flight motor with any specified

amount of slag in the chamber can be obtained from extrapolation (or interpolation). Apparently, if more test data at different motor spinning rates are available, analysis results will be more reliable in predicting the flight motor thermal environment with a specified amount of slag in the chamber. Since accurate determination of the amount of slag in the spinning flight motor chamber is a difficult task and is a subject of further study, the methodology presented here will be directly applicable to evaluating a motor-case thermal environment associated with a conservatively estimated ($+3\sigma$) amount of slag in the flight motor chamber.

IV. Ground Motor Test Data

Correlation with the temperature data based on the derived Q2 radiation heating rate results in the heating-rate enhancement factors shown in Fig. 6 for the qualification motors given in Table 1. Figure 7 shows the comparison of soak-out temperature history on the forward dome of the PAM motor from this analysis with that from the Q5 motor test data. The enhancement factor for the radiation heating rate from a reference Q2 motor [0.14-lb (0.06-kg) slag] to the Q5 motor [4.50-lb (2.0-kg) slag] is 2.0. The agreement between the results of analysis and test data is very good throughout the entire soak-out history. The peak temperature reached on the forward dome during heat soak for a 4.50-lb (2.0-kg) slag in the PAM motor chamber is 615°F (324°C). Shown in the same figure are the results from the analyses of Refs. 10 and 11, which use a constant slag temperature and a noncharring thermal analysis and fail to match the soak-out temperature history.

Similar good agreement between the computed and measured soak-out temperature history on the forward dome of the Q6 motor [9.50-lb (4.3-kg) slag] is illustrated in Fig. 8. The enhancement factor for the radiation heating rate from the reference Q2 motor [0.14-lb (0.06-kg) slag] to the Q6 motor [9.50-lb (4.3-kg) slag] is 2.222 (see Fig. 6). The peak temperature reached on the forward dome during heat soak for a 9.50-lb (4.3-kg) slag in the PAM motor chamber is 634°F (334°C). The measured temperatures for the Q6 motor (and other qualification motors) were wrongfully adjusted and reported [10,11] simply by subtracting the measured Q6 motor case tempertature[9] by 80°F (44°C) at every data point to reflect the change from an initial propellant temperature [110°F (43°C) for the Q6 motor] to a reference 30°F (−1°C). Figure 8 shows that the difference between the motor-case soak-out temperatures for the motor firing at 110°F (43°C) and at 30°F (−1°C) for the same motor action time is not constant throughout the duration of heat soak. Apparently, with the same amount of propellant in the motor chamber, the action time also will be different for the motor firing at different initial propellant temperatures. These wrongfully adjusted and reported data were used in Refs. 10 and 11 and in an earlier version of this study. The temperature data used in the present study are obtained from test data of Ref. 9, without any adjustment or modification.

With the boundary conditions discussed above and the heating-rate enhancement factors indicated in Fig. 6, the soak-out thermal environments computed from the present thermal model for all of the PAM qualification motors of Table 1 are shown in Figs. 9–11. Very good agreement between the analysis results and the test data from qualification motors at various motor spinning rates is obtained at all of the stations considered in Fig. 2. This demonstrates that the simple thermal model with the soak-out thermal environment determined by one single parameter, the slag mass, works well for correlating the temperature data obtained from the PAM qualification motor tests. For the PAM motor, the soak-out heating is found to be most severe on the forward dome of the motor case from the ground tests, because of thin rubber insulation thickness on the forward dome. On the aft dome of the motor case, the temperature vs time curve in Fig. 11 also shows the slope at the end of motor firing, which is used to derive the insulation erosion rate for the qualification motors. The computed peak temperatures are plotted in Fig. 6 for all of the qualification motors considered in this study. At each station, test data obtained from the thermocouples with the highest

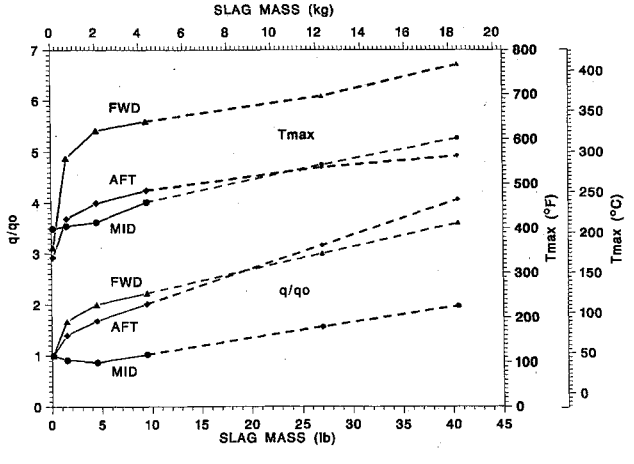

Fig. 6 Heating-rate enhancement factor and maximum temperature.

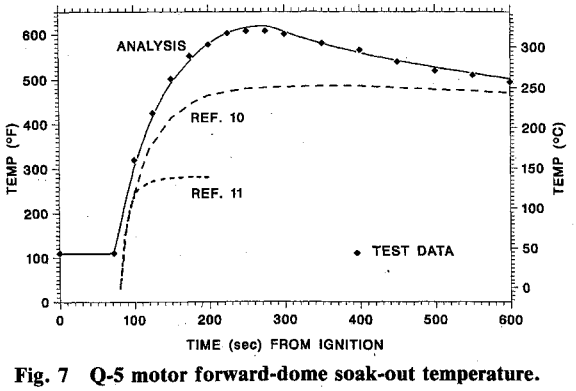

Fig. 7 Q-5 motor forward-dome soak-out temperature.

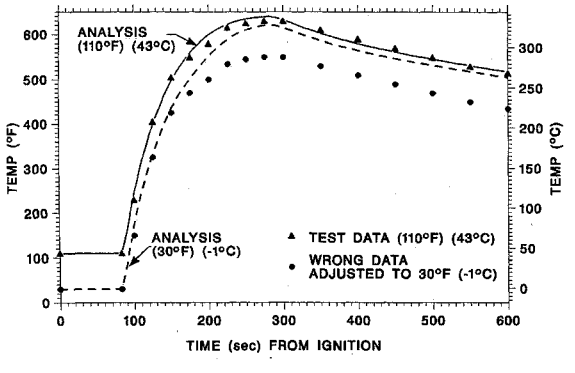

Fig. 8 Q-6 motor forward-dome soak-out temperature.

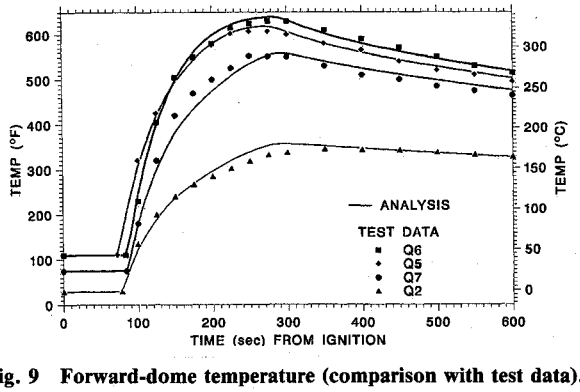

Fig. 9 Forward-dome temperature (comparison with test data).

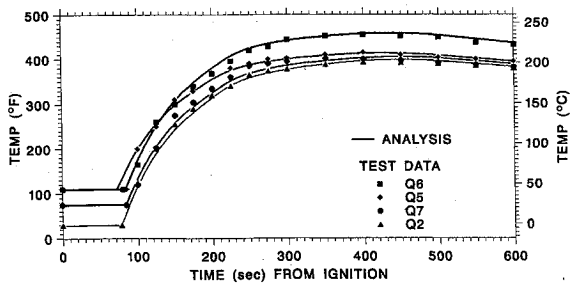

Fig. 10 Mid-dome temperature (comparison with test data).

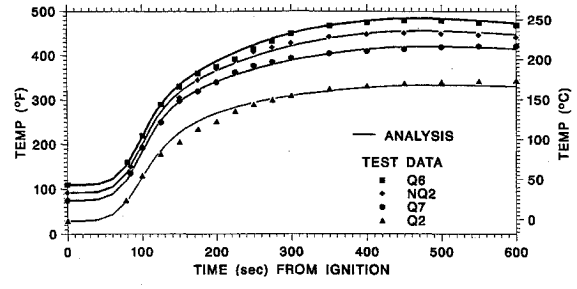

Fig. 11 Aft-dome temperature (comparison with test data).

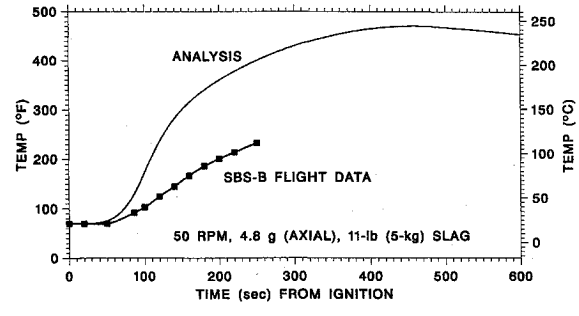

Fig. 12 SBS-B flight motor aft-dome soak-out temperature.

temperature reading are used for analysis comparison. These thermocouples are TC2, TC5, and TC14 at forward-, mid-, and aft-dome stations, respectively, which are specified in Ref. 9 and shown in Fig. 2.

Somewhat surprising results are noticed from temperature data correlation on the mid-dome of the qualification motors. The soak-out radiation heating rate decreases slightly with increased slag mass from 0.14 lb (0.06 kg) (Q2 motor) to 1.5 lb (0.7 kg) (Q7 motor) and 4.5 lb (2.0 kg) (Q5 motor) shown in Fig. 6. A possible explanation is that centrifugal force from motor spinning causes the slag to accumulate near the cylindrical portion of the motor; also, the solidified surface of the slag in the mid-dome area shields off radiation heating from other parts of the chamber and the nozzle during heat soak.

V. Flight Motor Data

From recovered flight strategic motors such as the Trident-I, Stages 1 and 2, and the Peacekeeper, Stage 1, more internal insulation erosion is observed on the forward dome of the motor case of a flight motor than that of the same motor tested on the ground. But on the aft dome, less insulation erosion is measured on the flight strategic motor than on the ground motor.[7] For the PAM-S/Ulysses motor, the forward-dome insulation is covered by the propellant and will not be exposed to hot combustion products until near the end of burn. Therefore, the flight enhancement of insulation erosion will not affect the PAM-S motor's forward-dome insulation design derived from ground motor data.

On the aft dome, the results of the present analysis for the Delta/PAM-D/SBS-B flight motor (50 rpm, 4.8 axial g), which was launched in September 1981, are compared with the flight temperature data [12] in Fig. 12. For this flight motor, the erosion rate is 2.5 mil/s (0.064 mm/s) from Fig. 4. Note that the aft-dome thermal environment is less severe on the flight motor than on the ground motor. To get a good match with the flight temperature data, significant reduction is required in both insulation erosion rate and heated surface temperature.

The benign thermal environment on the aft dome of the flight motor could be the result of the axial acceleration force that caused near-stationary spotty contact between alumina particles and EPDM. The charred EPDM layers were pressed against the motor interior surface. The retained EPDM char layers shielded off the radiation heating from other parts of the chamber. Without removal of the charred EPDM layers, the erosion rate is reduced significantly, and thermal penetration is less severe. The temperature data from the Delta/PAM-S/SBS-B flight motor indicate that the aft-dome temperature predicted from the present technique for a flight space motor is conservative. This can be viewed as less insulation erosion on the aft dome of the flight PAM motor, which is consistent with the result observed from the recovered flight strategic motors.

VI. Prediction for PAM-S/Ulysses Mission

An analysis method for accurate determination of the amount of slag in the chamber of a spinning flight motor is not yet well established. The nominal amount of slag retained in the motor chamber for the PAM-S/Ulysses mission was estimated[5] to be 27 lb (12.2 kg); and the worst case ($+3\sigma$) value was estimated to be 40.5 lb (18.4 kg). For the PAM-S/Ulysses mission (72 rpm, 90-s burn), the predicted temperature history on the outside surface of the motor case from the present analysis is shown in Figs. 13–15, which are obtained from the extrapolation of the heating-rate enhancement factors to these slag masses shown by the dash lines in Fig. 6. The peak soak-out temperatures on the motor case from the present thermal models also are shown in the same figure. A plot of q/q_0 vs the log of the slag mass (or the log of q/q_0 vs the log of the slag mass) will result in the heating rate–slag mass curve being closer to a straight line than that shown in Fig. 6. But the extrapolation based on linear-log (or log-log) plot will be less conservative than that shown in Fig. 6 for the PAM-S/Ulysses mission. For example, the extrapolation in Fig. 6 shows that at 40.5-lb (18.4-kg) slag, $q/q_0 = 3.6$ and 4.06 at the forward and aft dome, respectively; whereas the extrapolation in a linear-log plot will result in $q/q_0 = 2.65$ and 2.80 at the forward and aft domes, respectively.

Note from Fig. 6, for the motor case covered with MLI blankets, that the peak temperature for the $+3\sigma$ case [40.5-lb (18.4-kg) slag] of the PAM-S/Ulysses mission is 810°F (432°C) (770°F + 40°F) (410°C + 22°C) on the forward dome, from this analysis. Since the maximum allowable temperature for Kapton-based MLI is approximately 750°F (399°C), the use of high-temperature quartz cloth to cover the motor case (underneath the MLI blankets) will be helpful to maintain the integrity of MLI blankets and to reduce the possiblity of outgassing of Kapton at high temperature, which could contaminate the spacecraft. The titanium motor case, however, can tolerate a slag mass of 40.5 lb (18.4 kg) in the motor chamber, since the melting point of titanium is 3074°F (1690°C), and its usable temperature is above 1000°F (538°C) after motor burnout when the chamber pressure drops to a negligible value. The present analysis predicts no motor-case burn through, even for a $+3\sigma$ (40.5-lb) (18.4-kg) slag in the chamber of the PAM motor.

A remaining question to be answered is whether the PAM-S/Ulysses nozzle support structure will become "flexible" or "overheated" during motor firing or heat soak. A detailed two-dimensional thermal analysis for the Star-48 nozzle is given in Ref. 13. An improved method of analysis that considers charring and material ablation in a two-dimensional space can be found in Ref. 14 for the IUS small motor, and the same methodology can be applied to the PAM-S motor. How-

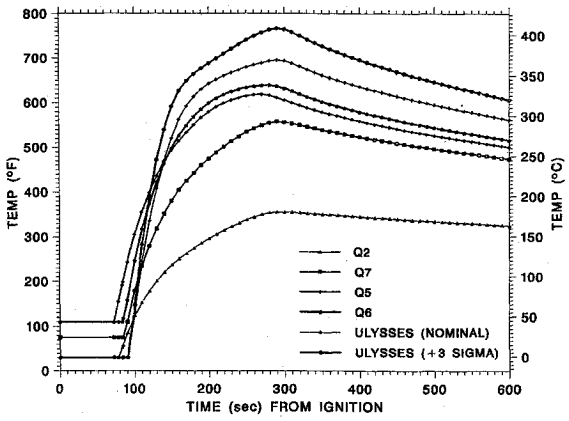

Fig. 13 Forward-dome soak-out temperature (analysis results).

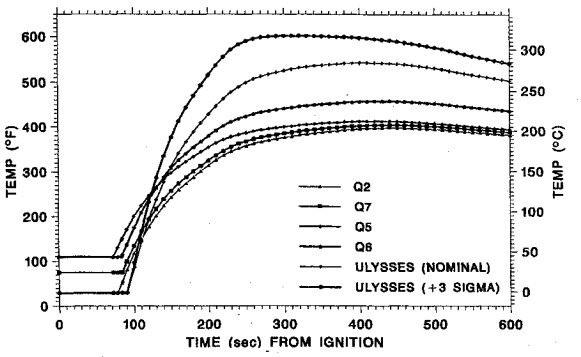

Fig. 14 Mid-dome soak-out temperature (analysis results).

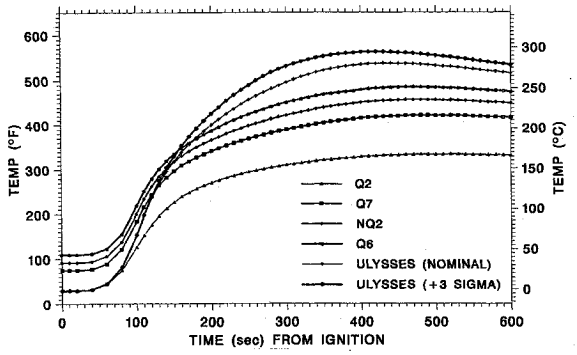

Fig. 15 Aft-dome soak-out temperature (analysis results).

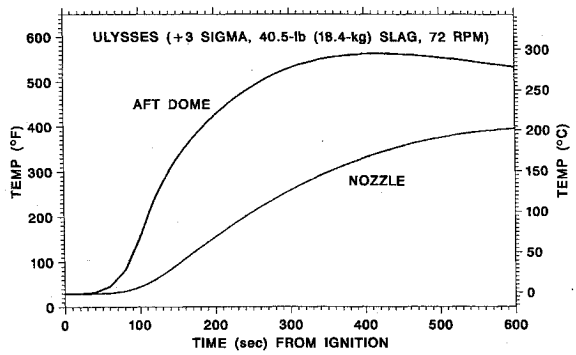

Fig. 16 Aft-dome and nozzle-closure temperature.

ever, for a qualitative assessment of nozzle thermostructural integrity due to the presence of slag in the motor chamber, similar one-dimensional thermal analysis as that for the motor case is carried out at the station with the thinnest EPDM insulation (0.55 in.) (1.4 cm) as indicated by the dashed line in Fig. 3, where the titanium nozzle closure thickness is 0.10 in. (0.25 cm). The EPDM erosion rate is 2.60 mil/s (0.07 mm/s) at 72 rpm from Fig. 4. With this erosion rate and the particle solidification temperature of 3720°F (2049°C) applied on the EPDM heated surface during motor firing and the radiation heating rate obtained from Fig. 6 [40.5-lb (18.4-kg) slag] during heat soak, the calculated temperature history of the titanium nozzle support ring is shown in Fig. 16. The maximum temperature at the titanium nozzle support ring stays cool at the end of burn and reaches 396°F (202°C) at 600 s from ignition. Shown in the same figure for comparison are the predicted aft-dome temperature histories for the PAM-S/Ulysses mission at this station with the thinnest EPDM insulation.

The analysis and results presented herein can be used to assess the amount of slag retained in the chamber, if the thermal environment of the forward dome is monitored during flight. To do so, the radiation-enhancement factor of Fig. 6 needs to be firmly established for the increased slag masses condition and derived from all of the available ground test data. This requires that some ground motor tests be carried out at higher rpm than that of the available motor tests. Ground motor tests conducted on a centrifuge in lieu of a high motor spinning rate will be helpful in retaining an increased amount of slag in the chamber. The relationship between the radiation-enhancement factor and slag mass for other motors with different chamber and grain design than that of the PAM motor may not be the same as that given in Fig. 6 and needs to be derived from motor test data. Once the radiation-enhancement factor and thermal environment associated with various slag masses in the chamber are established for a spinning ground motor, it will be an easy matter to apply the present thermal analysis technique for slag-mass assessment through a matching forward-dome, soak-out temperature history with that monitored from a flight motor. By the same token, the present thermal model also can be used for assessing the insulation erosion rate of a flight motor, if the thermal environment in the full exposure area, like the aft dome of the flight PAM motor, is monitored.

The present analysis needs to be backed by an effective means of determining where the slag pool is within the motor during firing. Analysis methods for solving gas-particle, two-phase, inviscid flows were given in Refs. 15 and 16. An efficient, finite-element method for solving Navier-Stokes flows inside solid rocket motors was presented in Ref. 17. Further study along this line for gas-particle, two-phase, viscous flows with radial acceleration (spinning rocket motor) and axial acceleration (flight motor) may provide accurate determination of the amount and location of the slag in the spinning flight motor chamber.

A prerequisite for a reliable prediction or assessment of a spinning flight motor thermal environment is an analysis method that is simple enough to use, yet provides analysis results in good agreement with the data obtained from available ground motor tests. The thermal model and correlation technique presented in this paper represents a macroscopic approach to a very complicated problem and falls into this category.

VII. Conclusions

Very good agreement between analysis results and ground test data for the motor-case temperature histories throughout motor firing and the heat-soak period of the spinning PAM qualification motors at various motor spinning rates is obtained from the simple thermal model developed in this study. In the area in which insulation is exposed to combustion products during motor firing, the insulation erosion rate is a function of the motor spinning rate. The slag mass is considered to be the single parameter which influences the chamber thermal environment during heat soak. The analysis predicts no motor-case burn through or nozzle-support ring thermostructural degradation for the PAM-S/Ulysses flight motor with 40.5-lb (18.4-kg) slag retained in the chamber. For a spinning flight motor, the study illustrates a way to assess the insulation

erosion rate during motor firing and the amount of slag accumulated in the chamber during heat soak, from monitoring or sensing the temperature on the outside surface of the motor case. To establish the applicable limit of the present correlation technique for much greater amounts of slag in the motor chamber than those shown in the paper, data obtained from tests conducted at high rpm and/or high acceleration are required.

Postscript

After the presentation of this paper at the AIAA/SAE/ASME/ASEE 26th Joint Propulsion Conference in Orlando, Florida, on July 17, 1990, the Orbiter/IUS/PAM-S/Ulysses was launched successfully from Launch Complex 39B, Kennedy Space Center, Cape Canaveral, Florida, on October 6, 1990. All flight objectives were satisfactorily met, based on preliminary evaluation of telemetered data.

Acknowledgment

This work was supported by the U.S. Air Force Space Systems Division under Contract F04701-88-C-0089.

References

[1]Motzko, M. O., "PAM-S Solid Rocket Motor Design Analysis Report," MDC H3517, SDRL 047, McDonnell Douglas Astronautics Company, Huntington Beach, CA, Dec. 1987.

[2]Counts, P. V., "PAM-S Flexible Nozzle Concern," NASA Marshall Space Flight Center FA51 (89-131), NASA/MSFC Letter to AFSC, Huntsville, AL, May 10, 1989.

[3]Harduvel, J. T., "Results of Slag-Induced Coning Divergence Analysis for the Ulysses PAM-D Mission," McDonnell Douglas Memorandum A3-J960-JTH- SS-M-8700733, Huntington Beach, CA, June 1987.

[4]Sevaston, G. E. (ed.), "Ulysses PAM-S Booster Nutation Control System Analysis," TR-1628-94(JPLD-6289), Jet Propulsion Lab., Pasadena, CA, Dec. 1989.

[5]Anon., "PAM-S Preliminary Design Review," MDC H3266, McDonnell Douglas Astronautics Company, Huntington Beach, CA, June 1987.

[6]Anon., "Aerotherm Charring Material Thermal Response and Ablation Program," Version 2, Edwards AFB, CA, AFRPL-TR-70-92, April 1970.

[7]Christensen, B. Y., and Daines, W. L., "Review of Flight Amplification Phenomena," Edwards AFB, CA, Rept. AFAL-TR-88-032, May 1988.

[8]Spencer, D. J., and Bixler, H. A., "Inertial Upper Stage Thermal Test Program," Air Force Space Systems Division, El Segundo, CA, Rept. SD-TR-89-26, April 1989.

[9]Anon., "Interim Report, Star-48 Qualification Program, Vol. I, Technical Discussion and Appendixes A-G, Subcontract 76917011," E98-81, Thiokol/Elkton Division, Elkton, MD, Oct. 1981.

[10]Motzko, M. O., "Attachment 1, MDAC-HB Thermal Analysis," *PAM-S Solid Rocket Motor Design Analysis Report,* MDC H3517, SDRL 047, McDonnell Douglas Astronautics Company, Huntington Beach, CA, Dec. 1987.

[11]Motzko, M. O., "Attachment 2, MTI Thermal Analysis," *PAM-S Solid Rocket Motor Design Analysis Report*, MDC H3517, SDRL 047, McDonnell Douglas Astronautics Company, Huntington Beach, CA, Dec. 1987.

[12]Strom, D. L., "PAM-S/Star-48B Thermal Analysis for the Soakback Period (with Slag)," A3-P927-PAM-88330, McDonnell Douglas Astronautics Company, Huntington Beach, CA, Sept. 1988.

[13]Reed, D. R., "PAM-48 TE-M-711 Motor Thermal Analysis," RDTM-687, Morton-Thiokol Inc., Elkton, MD, Aug. 1977.

[14]Chang, I.-S., "A Two-Dimensional Charring Thermal Analysis for IUS SRM-2 Nozzle Assembly," TOR-0086 (6464-02)-1, The Aerospace Corporation, El Segundo, CA, Feb. 1986.

[15]Chang, I.-S., "One- and Two-Phase Nozzle Flows," *AIAA Journal,* Vol. 18, No. 12, Dec. 1980, pp. 1455–1461; also AIAA Paper 80-0272.

[16]Chang, I.-S., "Three-Dimensional, Two-Phase, Transonic, Canted Nozzle Flows," *AIAA Journal*, Vol. 28, No. 5, May 1990, pp. 790–797; also AIAA Paper 88-3201.

[17]Chang, I.-S., "An Efficient, Intelligent Solution for Viscous Flows Inside Solid Rocket Motors," Paper 2D-1, 1990 JANNAF Propulsion Meeting, Anaheim, CA, Oct. 1990; CPIA-PUB-560, Vol. 2, p. 47, Applied Physics Laboratory, Laurel, MD; also AIAA Paper 91-2429.

James A. Martin
Associate Editor